DEMANDS ON NONSTRUCTURAL COMPONENTS IN BUILDINGS WITH CONTROLLED ROCKING BRACED FRAMES

Nathan Buccella[1], Lydell Wiebe[1], Dimitrios Konstantinidis[2], and Taylor Steele[1]

[1]Department of Civil Engineering, McMaster University, Hamilton, Ontario, Canada

[2]Department of Civil and Environmental Engineering, University of California, Berkeley, USA

Controlled Rocking Braced Frames (CRBFs) have been developed as a high-performance seismic force resisting system that can self-centre after an earthquake and avoid structural damage. A CRBF is designed to uplift and rock on its foundation, and this response is controlled using prestressing and energy dissipation devices that are engaged by uplift. Although CRBFs have been shown to have desirable structural performance, a comprehensive assessment of this system must also consider the performance of nonstructural components, which have a significant impact on the safety and economic viability of the system. The purpose of this paper is to evaluate the demands on nonstructural components in buildings with CRBFs in comparison to demands in a reference codified system, taken here as a buckling restrained braced frame (BRBF), as well as to identify which design parameters influence these demands. The responses of various types of nonstructural components, including anchored components, stocky unanchored components that slide, and slender unanchored components that rock, are determined using a cascading analysis approach, where absolute floor accelerations generated from nonlinear time-history analyses of each system are used as input for computing the responses of nonstructural components. The results show that the downside of maintaining elastic behaviour of the CRBF members is, in general, larger demands on nonstructural components compared to the BRBF system. These demands are not highly influenced by impact during rocking or by the supplemental energy dissipation provided, as the vibration of the CRBF in its higher modes is primarily responsible for the higher demands.

KEYWORDS

nonstructural components, controlled rocking braced frames, buckling restrained braced frames, floor spectra, sliding components, rocking components, higher mode effects, acceleration spikes

INTRODUCTION

Controlled rocking braced frames (CRBFs) have been developed as a high-performance seismic design solution due to their ability to minimize structural damage and residual drifts. Research has shown that CRBFs can meet seismic demands at and above a design level earthquake while maintaining their self-centering capabilities [Eatherton and Hajjar 2010; Ma et al. 2010; Roke et al. 2010]. CRBFs replace the braced bays of a conventional braced frame system with a frame that is intentionally allowed to uplift and rock about its toes, as shown in Figure 1. Once uplift occurs, resistance to the system overturning is provided by the weight carried by the CRBF and by prestressing tendons. Although CRBFs have the potential to carry the tributary gravity loads from the floor diaphragms [Gledhill et al. 2008; Mottier et al. 2018], the CRBFs considered in this study are assumed to be decoupled from the gravity loads of the floor diaphragms [Latham et al. 2013; Steele and Wiebe 2020]. Supplemental energy dissipation can be provided using devices that are engaged by uplift. The result is a system where residual drifts are nearly zero due to self-centering, seismic demands on the frame members are reduced due to the uplift, and permanently damaged energy dissipation devices can typically be replaced.

Although CRBFs have shown promise as a high-performance system, structural performance is not the only consideration in the overall assessment of the effectiveness of a seismic force resisting system. One area of research that has increased in prominence recently is the seismic response of nonstructural components, which have been shown to have a significant impact on seismic losses [Filiatrault et al. 2001; Taghavi and Miranda 2003; Miranda et al. 2012]. Therefore, in order to measure the true seismic resiliency of buildings featuring the CRBF system, the performance of nonstructural components must also be assessed.

The demands on nonstructural components in buildings with CRBFs cannot be assumed to be similar to those experienced in conventional braced frame seismic force resisting systems. Nonlinear time-history analyses and shake table testing have shown that CRBFs can experience a significant increase in frame member forces (relative to the forces

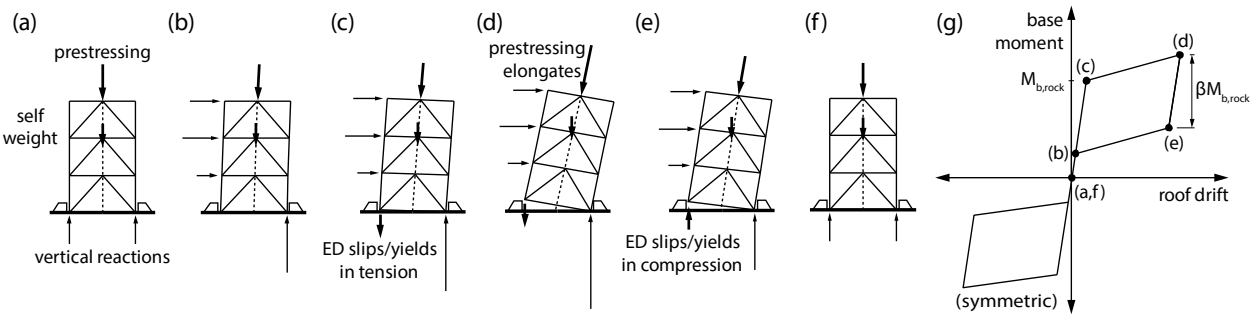

Figure 1 CRBF hysteretic response

calculated by a modal analysis of the frame using a design level spectral acceleration spectrum reduced by the overall force reduction factor, *R*, of the system) contributed by the frame vibrating in its higher modes during the rocking phase of the response [Eatherton and Hajjar 2010; Ma et al. 2010; Roke 2010; Wiebe et al. 2013]. Therefore, one concern for nonstructural component performance in CRBFs is whether these higher-mode forces will also translate to increased acceleration demands on nonstructural components.

Another concern for nonstructural components in CRBFs is potential spikes in floor acceleration or nonstructural component demand caused by column impact during rocking [Wiebe and Christopoulos 2010; Lin et al. 2012]. While vertical floor acceleration spikes at column impact are not expected for a decoupled CRBF system, lateral floor acceleration spikes are possible when the lateral stiffness of the system rapidly transitions from a low value during rocking to a high value upon column impact [Wiebe and Christopoulos 2010, Buchanan et al. 2011, Lin et al. 2012], though such spikes could not be identified during shake table testing [Wiebe et al. 2013]. Lin et al. [2012] showed that the demands on sliding contents in self-centering systems are not driven by the change from low to high stiffness but rather by the velocity at incipient sliding. The models of the structures in that study were limited to single degree-of-freedom oscillators, but further research in this area has been limited.

Dyanati et al. [2014] compared the structural and nonstructural performance of a six-storey CRBF with those of a conventional concentrically braced frame. They found that although the CRBF experienced better structural and drift-sensitive nonstructural performance than the concentrically braced frame, the demands on acceleration-sensitive nonstructural components were larger. Although the study provided insights into the relative performance of the two systems, the performance of drift-sensitive components was dependent on design decisions which could vary widely, and the assessment of acceleration-sensitive components was based only on peak floor accelerations. Pollino [2014] compared a three-storey CRBF to a buckling restrained braced frame (BRBF) structure and found that the floor spectra peaks in the CRBF were similar to those in the BRBF and that the floor spectra demands in CRBFs could be reduced by increasing the frame rigidity, thereby shifting the higher-mode periods away from high-energy content in the ground motions, or by allowing yielding in the frame members. However, the study was limited to a three-storey structure, and both approaches to reduce the floor spectra would come with structural disadvantages.

The purpose of this study is to provide a more comprehensive investigation of the demands on nonstructural components in CRBFs, including considering the influence of building height and of design decisions, and with special focus on the specific concerns that were discussed above for demands on nonstructural components in CRBFs. The analysis is based on buildings with three, six, and 12 storeys. For each building, two CRBFs are designed with different levels of energy dissipation, as well as one BRBF for comparison. The designs are iterated slightly to achieve similar median peak interstorey drifts, thus enabling direct comparison of the demands on acceleration-sensitive nonstructural components. The demands on nonstructural components are then analyzed using a cascading analysis approach. Three types of nonstructural components are considered: anchored components, assessed by means of elastic floor response spectra; unanchored stocky components, assessed by sliding displacement and velocity spectra; and unanchored slender components, assessed by rocking spectra.

DESIGN OF SEISMIC FORCE RESISTING SYSTEMS

Two CRBFs and one BRBF were designed for building heights of three, six, and 12 storeys. The structures were located in Los Angeles on site class D soil, as per ASCE 7-16 [2016]. The site had mapped MCE_R short- and 1-s period spectral accelerations of S_S = 1.5 g and S_1 = 0.6 g. The short-period site coefficient, F_a, and the long-period site coefficient, F_v, were 1.0 and 1.7, respectively. Figure 2 shows the structural layout of the gravity framing and the brace

configurations of the 3-storey CRBF and BRBF structures. The structure had equal storey heights of 4.57 m and equal bay widths of 9.14 m. The seismic weights of the floor and roof levels were 10,090 kN and 6,440 kN, respectively. Each CRBF consisted of a chevron braced frame that was designed to have a width of 80% of the bay width, so as to fit between the gravity columns on the column lines. Each BRBF consisted of two braced bays per frame with braces that extended the full width of each bay and were pinned to gusset plates at the beam-column joints. The number of frames used for each building height are shown in Tables 1 and 2 for the CRBF and BRBF systems, respectively.

Although the building was assumed to be a Risk Category II structure, a peak allowable seismic interstorey drift of 1.5% was chosen for the designs rather than the 2% allowable drift prescribed in ASCE 7-16 [2016]. The reason for this design choice was that if CRBFs are to be used as a high-performance system, designers are likely to also seek reduced demands on drift-sensitive nonstructural components.

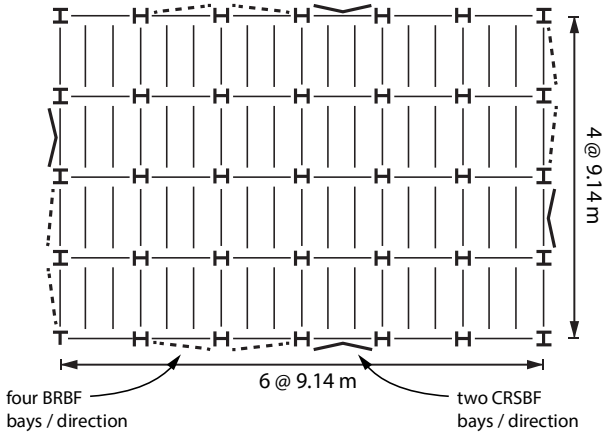

Figure 2 Floor plan for three-storey building

Controlled Rocking Braced Frames

The design methodology set out by Wiebe and Christopoulos [2015] was used to design the base rocking joints of the CRBFs based on selected values for the response modification factor R, the energy dissipation ratio β (see Figure 1), and the fundamental period of the CRBF before uplift. Each design was commenced using $R = 8$, as recommended by several researchers [Ma et al. 2010; Roke 2010; Eatherton et al. 2014], but this value was sometimes increased to achieve the same drift demands as in the BRBF designs, as discussed subsequently, based on other studies showing that CRBFs can meet drift and collapse criteria with larger values of R [Wiebe and Christopoulos 2015; Steele and Wiebe 2017]. Two different values of β (25% and 90%) were used for each building height, as listed in Table 1, in order to assess the influence of this parameter on the demands on nonstructural components. The ratio of the initial stress of the prestressing to the ultimate stress of the prestressing was targeted to be $\eta = 15\%$ for all CRBF designs, although this design objective needed to be altered for the 12-storey CRBFs, as discussed later. The fundamental period calculated from the OpenSees [PEER 2015] model described later was used in calculating the design loads.

The dynamic capacity design procedure developed by Steele and Wiebe [2016] was used to design the CRBF frame members. This procedure combines the force effects from the frame rocking to its ultimate base rotation in its fundamental mode with the force effects acting on the frame members due to higher-mode vibrations as the CRBF rocks. The higher-mode forces are computed using a model with modified boundary conditions to represent rocking, and resulting in the higher-mode periods $T_{2,rock}$ and $T_{3,rock}$ that are somewhat longer than the higher-mode periods with a fixed based model, as shown in Table 1. Although Steele [2019] found that considering the higher-mode force effects using the design spectrum without any amplification (i.e. $\gamma_{HM} = 1.0$) was adequate for preventing collapse, in this study, the design spectrum was amplified by $\gamma_{HM} = 2.0$ in an effort to ensure that frame member yielding or buckling was rare at the level of excitation for which nonstructural component demands were a concern.

Buckling Restrained Braced Frames

The BRBF structures were designed based on the equivalent lateral force procedure in ASCE 7-16 [2016] and the provisions of AISC 341-16 and 360-16 [2016]. In the initial design, R was taken as 8, and the fundamental period was

estimated based on the approximate fundamental period equation provided for BRBFs in ASCE 7-16 [2016]. After the initial design, if the target design drift criterion was not met, the effective R factor was reduced, and the new fundamental period was determined from the OpenSees model discussed subsequently. The BRBs were assumed to be pin connected to gusset plates at the beam-column connection of each braced bay. The three, six, and 12-storey BRBFs consisted of two frames with two braced bays in each frame. The BRB core areas were designed based on an assumed yield strength of 287 MPa. Although the BRB connections and gusset plates were not explicitly designed in this study, they were considered in the overall stiffness of the BRBs during design and modelling by assuming that the ratio of the actual length of the BRB core to the work point to work point distance of the hypotenuse of the braced bay was 0.68. The strain hardening and compressive strength adjustment factors were estimated based on the regression equations provided by Saxey and Daniels [2014], assuming that each BRB reached its probable tensile or compressive force at a strain that was twice the strain experienced by the BRB cores at the target design drift of 1.5%.

Design Iteration Based on Nonlinear Time-History Analysis

The designs of the seismic force resisting systems were iterated to reach similar median peak interstorey drifts based on the nonlinear time-history analyses, so that the demands on acceleration-sensitive components could be compared for systems with similar demands on drift-sensitive components. Following the design of each CRBF and BRBF, nonlinear time-history analyses were conducted, and if the largest median peak interstorey drift at any level was higher than the target design drift, or lower than the target design drift by more than 5%, the design was iterated by adjusting the design value of R. The ground motions were then rescaled and the time-history analyses repeated until the desired median peak interstorey drift was satisfied.

For the CRBFs, which are relatively stiff because of the capacity design process, this generally meant that the designs could be designed with a larger value of R while still achieving the drift target, especially when using a large amount of energy dissipation (β = 90%). However, the 12-storey CRBF with minimal energy dissipation required a reduced value of R, and the resulting prestressing force was very large, so the initial prestress was increased to η = 40%. Conversely, the 12-storey CRBF with β = 90% did not have a positive stiffness while rocking based on the area of post-tensioning needed to achieve η = 15%, so η was reduced to 9%.

For the BRBFs, achieving the drift target necessitated reducing the design value of R. For the taller frames, the nonuniform drift profile would have led to a very large overdesign to limit the drifts to 1.5% at all levels, so the design was iterated until the drifts at the lowest level were less than 1.5%, and other storeys where the drift still exceeded 1.5% were then manually overdesigned by no more than 16% to achieve the target drift.

The final design parameters for the CRBFs and the BRBFs are shown in Tables 1 and 2, respectively. Further details about the design of the CRBFs are given by Buccella [2019].

Table 1 CRBF design parameters

Design ID	Number of Braced Bays	R	β	η	# Strands	PT Location	T_1 (s)	T_2 (s)	T_3 (s)	$T_{2,rock}$ (s)	$T_{3,rock}$ (s)
3S-β25	2	10.32	25%	0.15	72	Middle	0.39	0.13	0.09	0.14	0.10
3S-β90	2	13.91	90%	0.15	33	Middle	0.48	0.16	0.12	0.18	0.13
6S-β25	4	17.78	25%	0.15	67	Middle	0.82	0.25	0.15	0.26	0.15
6S-β90	4	18.82	90%	0.15	33	Middle	0.94	0.29	0.16	0.30	0.17
12S-β25	4	5.25	25%	0.40	81	Columns	1.89	0.50	0.27	0.53	0.28
12S-β90	4	16.84	90%	0.09	46	Columns	2.26	0.55	0.29	0.60	0.30

Table 2 BRBF design parameters

Design ID	Number of Braced Bays	R	T_1 (s)	T_2 (s)	T_3 (s)
3S	4	5.41	0.72	0.32	0.20
6S	4	5.18	1.25	0.50	0.32
12S	4	4.30	2.27	0.84	0.49

MODELLING OF THE SEISMIC FORCE RESISTING SYSTEMS

An OpenSees [PEER 2015] model was used for the nonlinear time-history analyses of the CRBF system. An example schematic of the CRBF model for the three-storey structure is shown in Figure 3 (a). The beam, column and brace members were modelled using elastic beam-column elements. An elastic model of the frame members was deemed acceptable because the capacity design procedure ensured that for the majority of ground motions, the frame members remained elastic during the nonlinear time-history analyses. The stiffness provided by the gusset plate connections at the beam-column-brace joints was modelled using rigid elements. Although the brace members were assumed to be pin-connected to the rigid links of the gusset plates in the calculation of out-of-plane buckling loads, in the 2D model this connection was modelled as fixed in plane. A leaning column was modelled to capture the P-Delta effects acting on the system. The lateral inertial loads were assumed to be transferred from a rigid floor diaphragm to the CRBF at the centre nodes of the frame where the chevron braces meet. Therefore, the floor masses were lumped at the nodes of the leaning columns at each storey and the centre joints of the rocking frame were constrained in the horizontal direction to the leaning column nodes. The prestressing was modelled using a corotational truss element, combined with an initial stress material in parallel with a multi-linear material with a yield strain of 0.0083 and yield stress of 1670 MPa. The ultimate strain and stress of the prestressing were 0.013 and 1860 MPa, respectively. Depending on the location of the prestressing, the prestressing element was attached to either the centre node of the chevron braces or the beam-column-brace joint at the designed storey. The prestressing was anchored to the foundation using a tension-only gap element that prevented the prestressing truss element from developing compression stresses after yielding. The friction interface energy dissipation devices were located at the column bases and modelled using an elastic perfectly plastic element with an essentially infinite initial stiffness. Elastic-no tension horizontal and vertical gap elements that were essentially rigid in compression provided the foundation supports to the frame while also allowing it to uplift freely. A tangent stiffness-proportional Rayleigh damping model was used by applying an inherent damping ratio of 2% to the first two modes of the CRBF. Full details of the modelling approach can be found in Steele and Wiebe [2016].

The BRBFs were also modelled in OpenSees [PEER 2015], and a schematic of the model is shown in Figure 3 (b). Similar to the CRBF, the columns were modelled as continuous, with elastic beam-column elements and rigid offsets mimicking the gusset plate beam-column-brace connections. The beams were modelled as axially rigid in order to represent the assumed rigid floor diaphragm. A leaning column was also provided and was connected to the frame through axially rigid truss elements. The BRBs were modelled to match the equivalent stiffness and probable forces discussed earlier, using truss elements that were pinned to the beam-column-brace joints of the frame. The hysteretic response of the BRBs was modelled using the Steel02 material in OpenSees, calibrated based on the results of the regression equations developed by Saxey and Daniels [2014]. The post-yielding stiffness was modelled as 2% of the initial stiffness, and the final isotropic hardening parameters in tension and compression were 0.032 and 0.066, respectively. Further discussion and validation of the model is provided by Buccella [2019].

MODELLING OF THE NONSTRUCTURAL ELEMENTS

The three types of components studied were acceleration-sensitive anchored components, unanchored sliding components, and unanchored rocking components, as shown in Figure 4. In all cases, a cascading analysis approach was used to obtain the response of each component by applying the absolute floor accelerations obtained from the

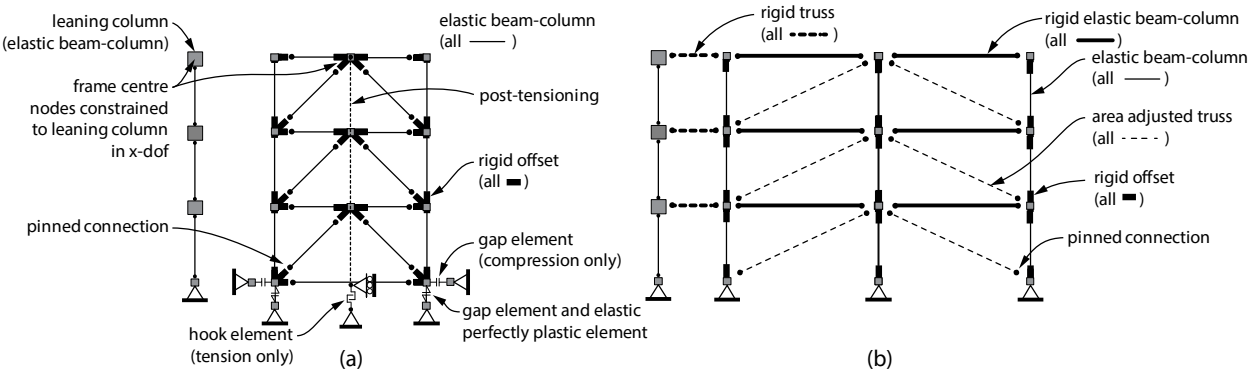

Figure 3 OpenSees model schematics: (a) CRBF [after Steele and Wiebe, 2016], (b) BRBF

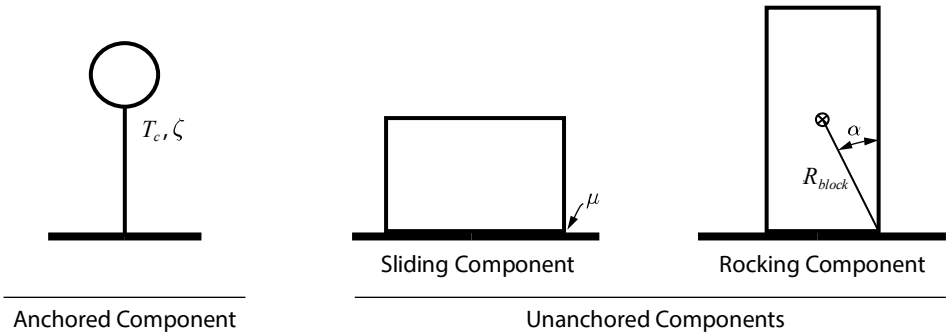

Figure 4 Idealized anchored and unanchored nonstructural components

nonlinear time-history analyses at each storey level to a model of each component. Because the CRBFs analyzed in this study were designed as decoupled from the gravity system, vertical accelerations caused by the CRBF uplifting and rocking are not expected to be transferred to the floor diaphragms [e.g. Wiebe et al. 2013], and therefore only lateral floor accelerations were considered in this study.

The performance of acceleration-sensitive anchored components was assessed by means of elastic floor spectra of peak pseudo-acceleration, defining the natural period of the anchored component as T_c and assuming a viscous damping ratio of $\zeta = 2\%$.

A rigid block that was free, and stocky enough, to slide without rocking was used to determine the demands on sliding components. The block was subjected to the absolute accelerations of each floor. A Coulomb friction model was used to characterize the interface between the block and the floor. The static and kinetic friction coefficients were assumed to be identical, as previous studies have shown that considering the difference between the static and kinetic coefficients of friction in the Coulomb friction model does not have a major impact on peak sliding displacements [Chaudhuri and Hutchinson, 2006; Konstantinidis and Makris, 2009]. Friction coefficient μ values in the 0.05 to 0.8 range were considered. The equation of motion of the sliding block was solved using standard ODE solvers in MATLAB [2017] and an event locator for detecting when the block was stuck to the floor or continued its motion. The demands on the sliding building components are presented as *sliding spectra* [Lin et al. 2015; Van Engelen et al. 2016], which show the peak sliding displacements (or velocities) of the components versus their friction coefficients.

The seismic demands on unanchored slender contents were computed using the model of a pure-rocking rigid block proposed by Housner [1963]. Although unanchored components may exhibit a combination of sliding and rocking [Bao and Konstantinidis 2020], the consideration of this coupled response is beyond the scope of this study. As such, it was assumed that for slender components, the interface between the floor and the block had sufficient friction to prevent sliding. Absolute floor accelerations were applied to the rocking block of size R_{block} and slenderness angle α (see Figure 4). The equation of motion for the rotation of the block θ, developed by Housner [1963], was solved using standard ODE solvers in MATLAB [2017]. An event locator was used, which detected when the block reached zero rotation (impact). A coefficient of restitution, e, was used to represent the energy lost during impact. When impact was detected, the post-impact angular velocity was computed by multiplying the pre-impact angular velocity by the value of $e = 1 - 1.5 \sin^2(\alpha)$ [1963]. Rocking components with three different slenderness angles, 10°, 15°, and 20°, at block sizes ranging from $R_{block} = 0.2$ m to 2.0 m were analyzed. The demands on the rocking components are presented as *rocking spectra* [Makris and Konstantinidis 2003; Dar et al. 2016], which are curves showing the normalized peak rotation, θ / α, of rocking blocks with constant slenderness α versus their size R_{block}. A ratio of $\theta / \alpha = 1$ represents overturning.

GROUND MOTION SELECTION AND SCALING

The FEMA P695 far-field record suite of 44 ground motions [ATC 2009] was used in the nonlinear time-history analysis. After applying the peak ground velocity normalization factors provided in FEMA P695, the suite was scaled by a single scale factor for each building height that would minimize the mean squared error of the median spectral acceleration of the suite compared to the design earthquake (DE) spectrum over a period range of 0.2 times the smallest of the fundamental periods of the three designs to twice the largest of the fundamental periods of the three designs. This was a modification of the scaling method suggested in ASCE 7-16 [2016] to allow comparison of demands across

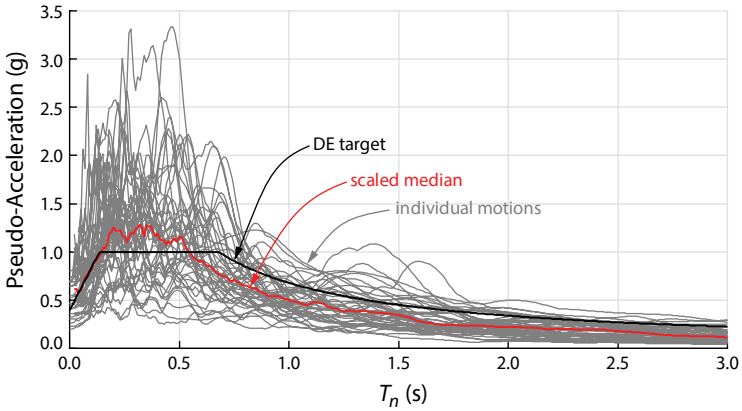

Figure 5 Design response spectrum and scaled ground motions for three-storey buildings

different designs for the same ground motions. The scale factors for the three-, six-, and 12-storey structures were 1.43, 1.49 and 1.68, respectively, and an example of the scaled response spectra is shown in Figure 5. No vertical components of ground excitation were applied.

STRUCTURAL RESPONSE

The interstorey drift profiles, residual interstorey drifts and brace forces for the three-, six-, and 12-storey structures are shown in Figure 6. The fundamental rocking mode dominates the displacement response of the CRBFs. This is evident especially in the nearly uniform drift profiles of the three- and six-storey CRBFs. As the height of the CRBF increases, the rocking frame becomes more flexible, and, although the rocking mode still dominates the displacement response, the deformations of the frame members contribute more to the interstorey drifts. Conversely, the BRBFs experience a much less uniform drift profile, where interstorey drifts tend to concentrate at the lower and upper storeys, even though yielding occurred at all storeys at the DE intensity. The uniform drift profile of the CRBF could be seen as an advantage because of the lack of drift concentration and because the designer has more control over reducing the drifts of the CRBF, as increasing the rocking moment of the system may result in marginal changes in system cost, whereas greatly increasing the stiffness of the BRB cores may be unfeasible. At the same time, the non-uniform drift profile of the BRBF could also be seen as an advantage, as only a few of the storeys would experience demands on drift-sensitive nonstructural components that reach the design limit.

As expected, the self-centering capabilities of the CRBF made the residual displacement of the system essentially zero at the DE intensity. Conversely, for the BRBF structures, the largest median residual interstorey drifts experienced at any storey were 0.38%, 0.34%, and 0.39% for the three-, six-, and 12-storey structures, respectively. Furthermore, the percentage of ground motions that caused at least one storey to experience a residual drift of greater than 0.5% (a value that can suggest it is more feasible economically to completely demolish and reconstruct the structure [McCormick et al. 2008]) was 45%, 50%, and 66% in the three-, six-, and 12-storey BRBFs, respectively. The large percentage of ground motions with excessive residual drifts in the BRBF is significant in comparing the overall performance, as demands on nonstructural elements may not have a significant impact on the expected seismic losses of the building if significant reconstruction or demolition is necessary.

Figure 6 also shows the peak compressive force experienced in the CRBF braces at each storey, along with the corresponding capacities. The results show that the capacity design procedure was successful in ensuring the braces remained elastic during 84% of the nonlinear time-history analyses, with the exception of the 12-storey design with $\beta = 25\%$, where 30% of the ground motions would have caused brace buckling. As such, the median results presented below are not adversely affected by using a model with elastic beam-column brace elements. Finally, the hysteretic responses of the first storey BRBs are also shown in Figure 6 for ground motions that produced near-median interstorey drift demands at the DE intensity. The results show that the BRB cores experienced significant yielding at this level, whereas at ¼ DE intensity there was little to no yielding at the first storey.

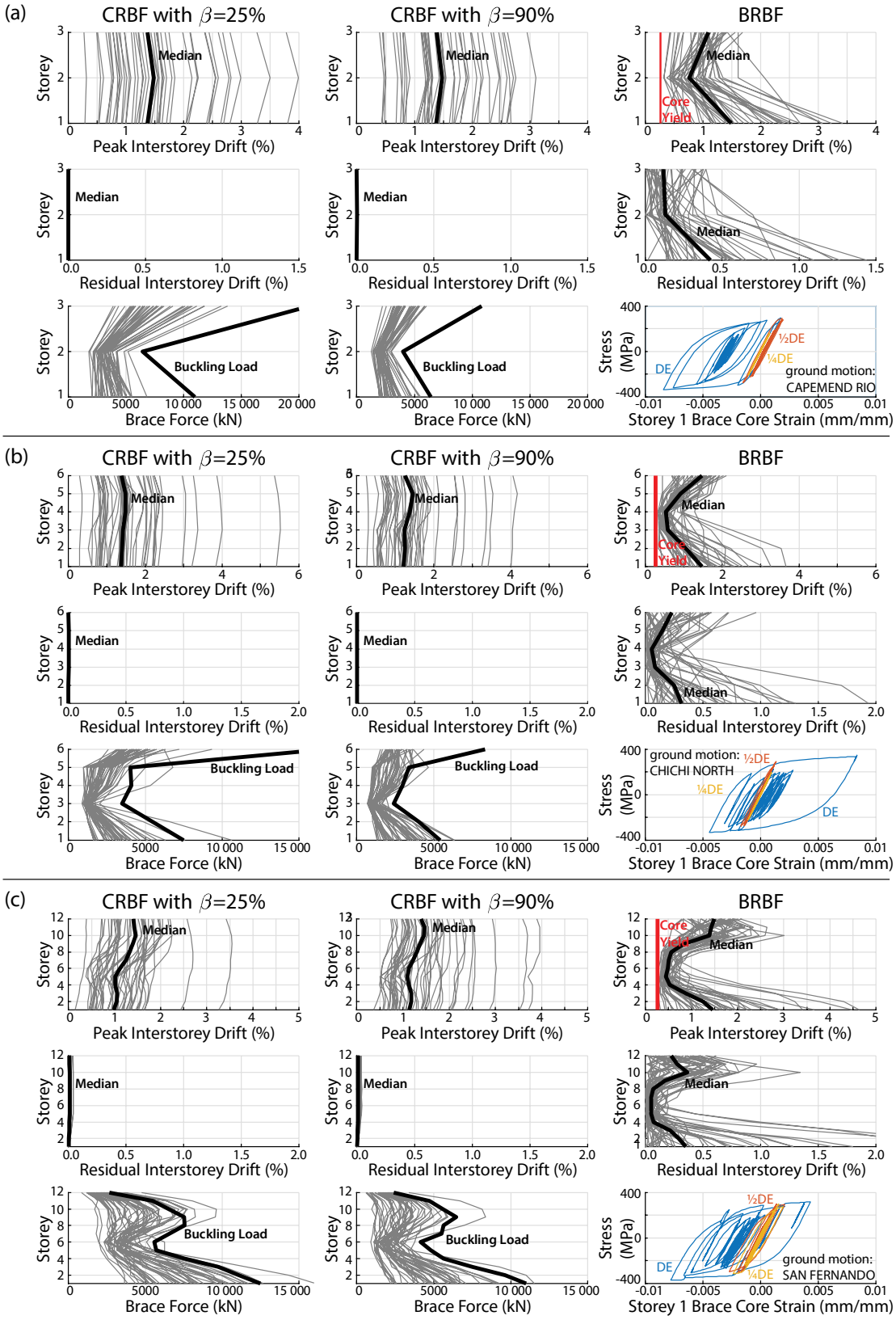

Figure 6 Nonlinear time-history analysis structural results for CRBFs and BRBFs with: (a) three storeys, (b) six storeys, and (c) 12 storeys

DEMANDS ON ACCELERATION-SENSITIVE ANCHORED COMPONENTS

Rigid acceleration-sensitive anchored components

For anchored components that are considered rigid (i.e. periods of less than 0.06 s [ASCE 2016]), the floor spectra shown later were relatively flat in the 0 to 0.06 s period range, except for one of the three-storey CRBFs that may have been influenced by the proximity of the third-mode period to this range. Therefore, peak floor accelerations (PFAs) were deemed an acceptable measure of rigid anchored component demands for both systems. Figure 7 compares the median PFAs at different building heights and earthquake intensities between the two systems. At the DE level for all building heights, the PFAs in the BRBF were typically lower than in the CRBFs, regardless of the amount of energy dissipation provided. Also notable was that at the DE intensity, the elongation of natural periods in the BRBF does not allow a magnification of the peak ground acceleration (PGA) over the height of the structure, whereas in the CRBFs the PFAs were typically magnified compared to the PGA. The average of the median PFAs were typically larger than at least 0.64 g in the CRBFs but were only around 0.4 to 0.5 g in the BRBFs, over all building heights. When comparing CRBFs of the same height with different levels of energy dissipation, the three- and 12-storey CRBFs experienced lower PFAs in the design with more energy dissipation, but the six-storey CRBFs experienced nearly identical average PFAs.

At the DE level, the average of the median PFAs in both CRBFs were 32%-39% larger than the PGA, depending on the building height, whereas the average PFAs were 19%-23% lower than the PGA for the BRBFs. However, this difference was greatly reduced at ½ DE compared to the DE level, and at the ¼ DE intensity, the PFAs were similar between the two systems, with differences of less than 0.06 g in average median PFAs. The PFAs in the BRBF also follow a more linear distribution over the height of the buildings, indicating that the first-mode response drives the PFAs, whereas the PFAs in the CRBFs seem to be more affected by the higher modes of the frame since the distribution tends to take the shapes of higher modes, particularly the third.

Flexible acceleration-sensitive anchored components

In order to assess the performance of anchored components that are not considered to be rigid, the median peak pseudo-accelerations at DE and ¼ DE intensity levels for all heights of CRBF and BRBF structures are shown in Figure 8. The vertical lines represent the natural periods of each of the structures, using the fixed-base elastic model for the first

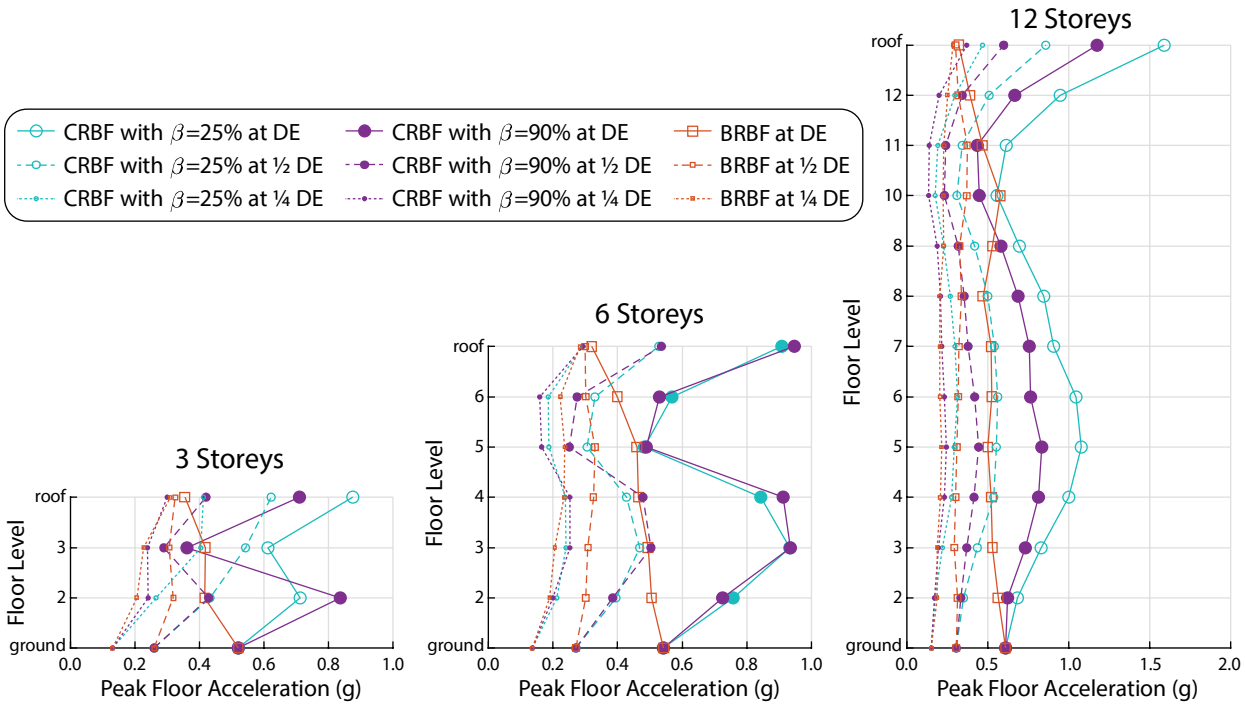

Figure 7 CRBF and BRBF median peak floor accelerations at DE, ½ DE and ¼ DE

mode but showing $T_{2,rock}$ and $T_{3,rock}$ instead of T_2 and T_3 for the CRBFs. Figure 8 shows that the spectral peaks of the CRBFs generally exceeded at least 4 g near the second- and third-mode periods calculated using the model with modified boundary conditions to simulate rocking. These peaks were typically at least twice as high as in the BRBF, and much larger than the peaks at or beyond the first-mode period of the CRBFs. In contrast, while the largest magnitudes in floor spectra of the BRBF occurred near the natural periods of the structure, these peaks were much more distributed than in the CRBF. This capping and spreading effect on the pseudo-accelerations is attributed to the elongation of periods in the BRBF due to yielding. At larger component periods, the pseudo-accelerations became either similar or larger in the BRBF, and then larger once again for the CRBFs with lower energy dissipation at periods beyond 1 s. These observations are relevant to the performance of very flexible or vibration isolated components, which can have natural periods greater than 1 s, but are beyond the range of periods for most anchored components, as even the most flexible anchored components are estimated to have natural periods in the range of 0.13 s for mechanical equipment and 0.3 s for electrical equipment cabinets [ASCE 2016]. These results suggest that specific attention should be paid to anchored components in CRBFs, particularly noting that the component amplification factor between 1.00 and 2.50 provided in ASCE 7-16 [ASCE 2016] for a variety of different nonstructural components would likely underestimate the magnitudes of pseudo-acceleration that would be experienced for anchored components in a CRBF.

The comparison of the performance of acceleration-sensitive anchored components changed when the intensity was reduced to 1/4 of the DE. In the CRBFs, the large spikes in pseudo-acceleration near the second- and third-mode periods reduced significantly. Although a reduction in floor spectra was also noticeable in the BRBFs, the reduction was not as significant. Instead, the BRBF floor spectra at ¼ DE began to resemble the CRBF floor spectra, with more defined peaks at the periods of the structure. Referring to the hysteretic response of the first-storey BRB shown in Figure 6, at ¼ DE the BRBF experienced minimal yielding, thus limiting the spreading and capping effect that was seen at the DE level. This was a common trend in the floor spectra, as the structural benefit of maintaining an elastic response resulted in higher magnitudes in floor spectra. However, due to the longer fundamental period of the designed BRBF structure, the CRBFs experienced their peaks in floor spectra at shorter periods, which may dominate the range of periods for most anchored components.

For taller structures, the participation of the higher modes of the CRBF resulted in relatively larger differences in floor spectra magnitudes between the two systems, with peaks that reached or exceeded about 8 g at multiple levels for both the six- and 12-storey CRBFs. Comparing the concentration of the floor spectra peaks to the BRBF structure at ¼ DE suggests that these peaks were caused by the CRBFs vibrating in their elastic modes throughout the excitation, rather than the CRBF having a significantly larger contribution of the higher modes than the BRBF structure.

Despite the large differences in supplemental energy dissipation provided to the two CRBFs at each height, the peaks in pseudo-acceleration were not consistently smaller in the β = 90% CRBF designs. For the three- and 12-storey CRBFs, although the peaks were typically slightly smaller for the β = 90% CRBF designs, the opposite was also the case at other floors and anchored component periods. When examining the floor spectra for the six-storey building, although the locations of the peaks differed, the magnitudes of the peaks were very similar between the β = 25% and β = 90% CRBF designs. Therefore, a comparison of the floor spectra for the two different CRBF base rocking joint designs but having identical capacity designed frames is shown in the following subsection to clarify the influence of the base rocking joint design and frame stiffness on CRBF floor spectra performance.

Comparison of floor spectra in different CRBF designs

As noted above, although the CRBFs designed with more energy dissipation (β = 90%) generally had slightly lower PFAs and spectral pseudo-accelerations than the designs with less energy dissipation (β = 25%), the differences were generally small and inconsistent, especially for the 6-storey CRBF. This was a surprising observation considering the large difference in supplemental damping, β, a parameter that is often considered to play an important role in reducing seismic forces and accelerations. Therefore, to further investigate the influence of the base rocking joint design and frame stiffness of the CRBFs on floor accelerations, nonlinear time-history analyses were also performed on two CRBFs for each building height with identical post-tensioning and energy dissipation as the previous designs, but both using the stiffest capacity designed frame (i.e. the design with β = 25%).

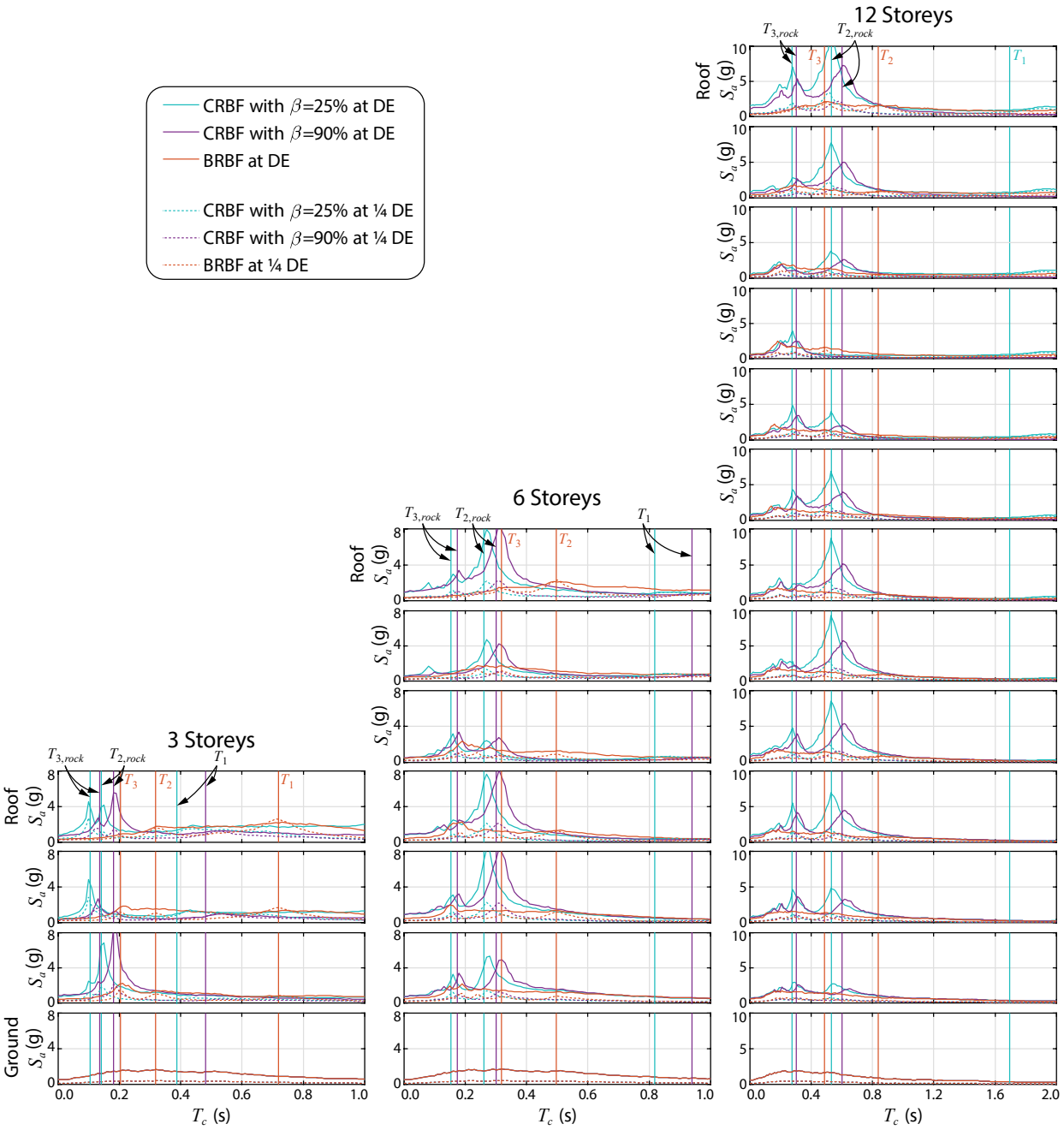

Figure 8 Median pseudo-acceleration floor spectra with 2% damping in the three-, six-, and 12-storey buildings with CRBFs and BRBFs

Figure 9 shows the resulting floor spectra of the CRBFs with identical frame members but differing post-tensioning and energy dissipation, along with the original $\beta = 90\%$ CRBF floor spectra, for the three-, six, and 12-storey buildings. For the three- and 12-storey buildings with identical frames, the CRBFs with more supplemental energy dissipation reach slightly lower peaks in pseudo-acceleration, but the differences in floor spectra are nearly negligible for the two six-storey base rocking joint designs with identical frame stiffness. With reference to Table 1, the six-storey CRBF designs had very similar effective force reduction factors, whereas the three- and 12-storey CRBFs with β = 90% had values of R that were much larger than the designs with β = 25%. This suggests that the amount of supplemental energy dissipation has a minimal influence on floor spectra magnitudes, particularly in the range of the higher modes

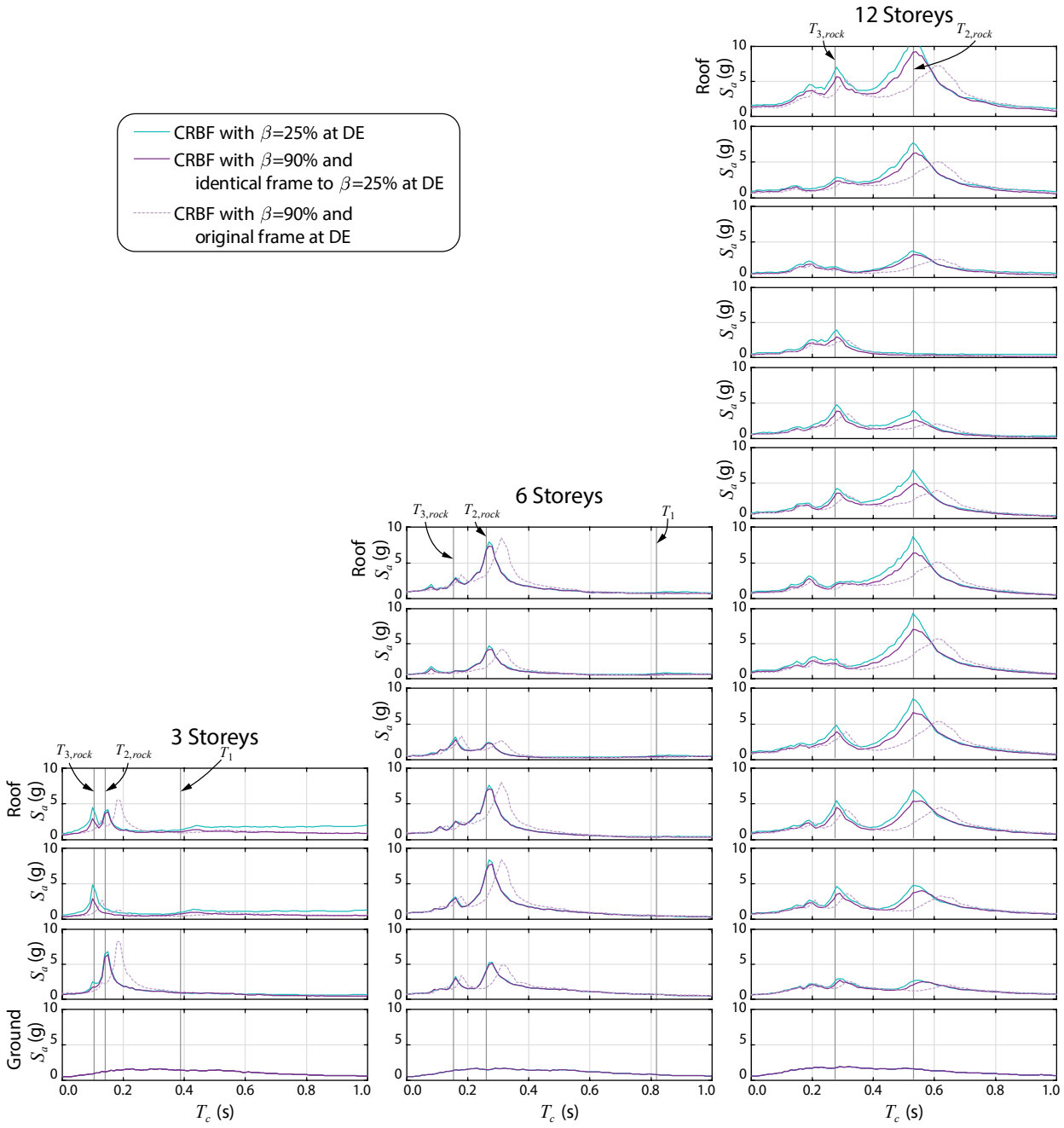

Figure 9 Median pseudo-acceleration floor spectra with 2% damping in the three-, six-, and 12-storey CRBFs designed with identical frames

of the frame, whereas the rocking moment of the CRBF influences the demands on anchored nonstructural components, as CRBFs that were designed with lower rocking moments had somewhat lower PFAs and floor spectra when considering designs with identical frame stiffness. Although more yielding, and therefore more energy dissipation, had a spreading and capping effect on the BRBF floor spectra, the energy dissipation provided in the CRBF is applied through a device that is engaged only through uplift, which is governed by the fundamental rocking mode of the frame [Wiebe et al. 2013], and therefore has a minimal impact on altering the higher modal properties of the frame.

DEMANDS ON UNANCHORED SLIDING COMPONENTS

Figure 10 shows median sliding displacement and velocity spectra for each floor in the buildings with CRBFs and BRBFs. The sliding spectra show that, with few exceptions, the buildings with CRBFs led to larger sliding displacements and velocities at the DE level than the building with BRBFs. Of the three building heights, the difference in average sliding displacement and velocity demands between the CRBFs and BRBFs was the largest for the 12-storey structures. The differences in sliding velocities between the two systems were generally more pronounced than the differences in sliding displacements.

For larger coefficients of friction ($\mu \geq 0.4$), unanchored components in the building with BRBFs generally did not experience any sliding at median levels, whereas such unanchored components in both buildings with CRBFs typically experienced sliding. For smaller values of μ ($0.05 \leq \mu \leq 0.35$), although the sliding spectra results seemed to follow the general trend of the PFAs that was shown in Figure 7, with the BRBF experiencing the least sliding followed by the $\beta = 90\%$ CRBF and then the $\beta = 25\%$ CRBF, the differences in peak sliding displacement and velocity were much smaller than the differences in PFA. For example, at the roof level of the three-storey buildings, the average sliding displacement in the $\beta = 90\%$ CRBF for $\mu \leq 0.35$ was only 11% larger than the average sliding displacement in the building with BRBFs, despite a PFA that was twice as large. These results suggest that PFAs are not a strong indicator of peak sliding response. Past research [Konstantinidis and Makris 2009; Konstantinidis and Nikfar 2015; Nikfar and Konstantinidis 2017] has shown that for analytical pulse excitations, sliding component response correlates better with the *persistence* of the excitation, which is a characteristic length scale of the excitation that is affected linearly by the strength of excitation (PFA) and quadratically by the period of the excitation. This is consistent with the increase in sliding demands in the buildings with CRBFs due to higher PFAs being mitigated by their shorter fundamental period relative to the buildings with BRBFs.

When comparing only the CRBFs, at the three- and 12-storey building heights, the $\beta = 90\%$ CRBF designs typically had lower median sliding displacements and velocities than the $\beta = 25\%$ CRBF designs. However, for the six-storey building, the sliding component performance was generally very similar when comparing the two CRBF designs, which is consistent with the similar PFAs and floor spectra peak magnitudes. Similarly, although the stiffness of the frame and its higher-mode vibrations appear to be the main influencers of nonstructural component performance in the CRBF buildings, the results from the sliding component analysis reinforce the observation that the R value of the CRBFs has some influence on nonstructural component demands, where designs with a lower rocking moment typically experienced lower sliding displacements and velocities.

When the earthquake intensity was reduced to ¼ DE, the sliding displacements and velocities were generally comparable or lower in the CRBF buildings compared to the BRBF buildings, even though the PFAs at ¼ DE were slightly larger in the CRBFs. This also was consistent with the observation that the persistence of the excitation, related to the longer period of the BRBF buildings, influenced the sliding demands. Nevertheless, the amount of sliding at this intensity was minimal, and in general at the median level there was negligible sliding for $\mu \geq 0.2$, which would govern many sliding building contents [Konstantinidis and Makris 2009, 2010].

DEMANDS ON UNANCHORED ROCKING COMPONENTS

Figure 11 shows rocking spectra for the three-, six-, and 12-storey structures. Relative to the acceleration-sensitive anchored component and sliding component performance results, the demands on rocking components at the DE level were more alike between the buildings with CRBFs and BRBFs. The most slender blocks ($\alpha = 10°$) overturned for almost all block sizes in both systems. For blocks with $\alpha = 15°$, the peak rotations were generally similar between the two systems, with the CRBFs producing smaller rotations at some floor levels in some building heights, and the BRBFs producing smaller rotations in other cases. The stockiest rocking component ($\alpha = 20°$) generally had smaller rotations in the buildings with BRBFs. While the trends in rocking spectra comparing the varying designs and block slenderness angles were typically similar across all three building heights, the 12-storey structures saw overturning of rocking components begin at slightly larger block sizes, followed by the three-storey structures and finally the six-storey structures.

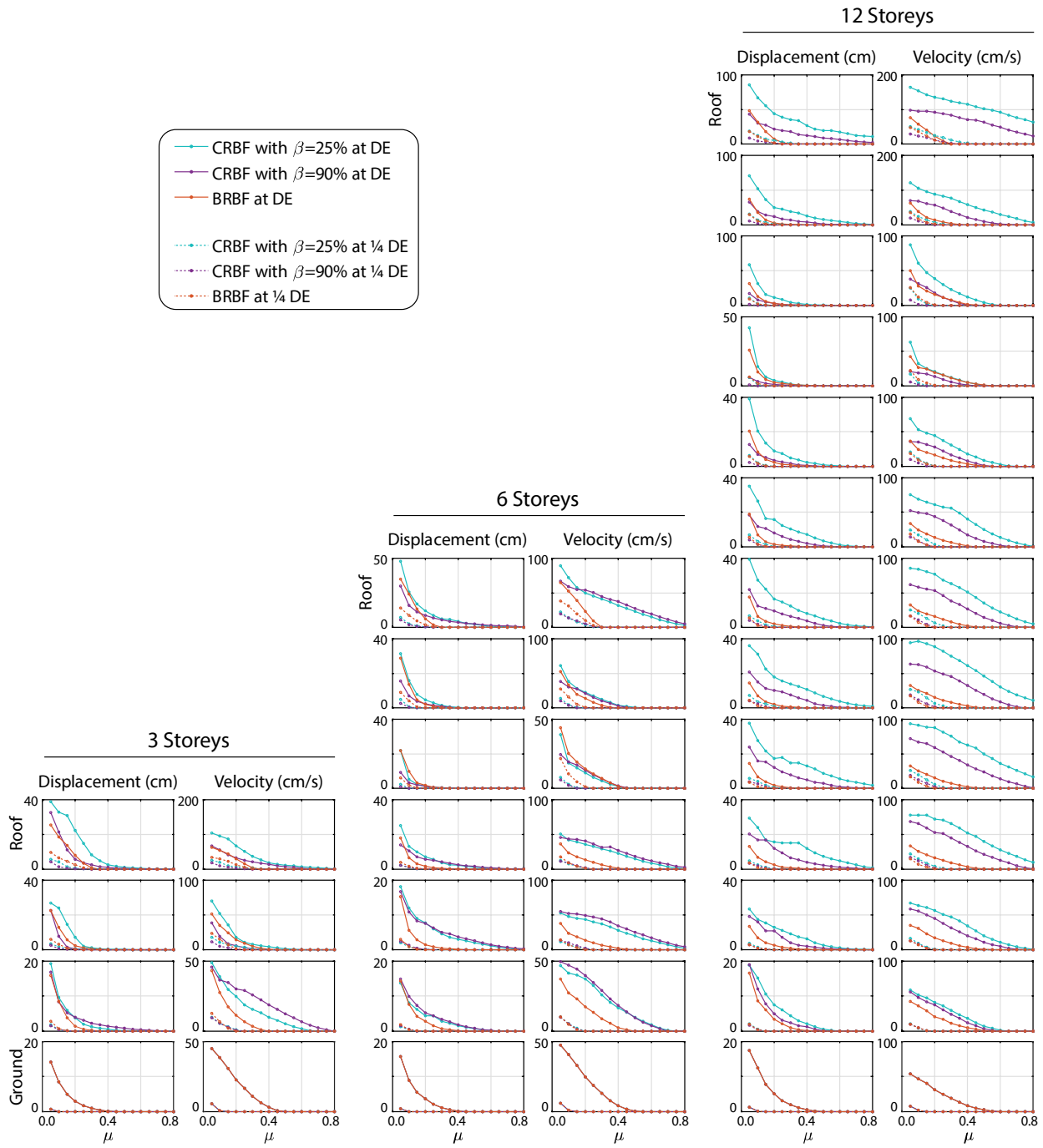

Figure 10 Median displacement and velocity spectra for unanchored sliding components in the three-, six-, and 12-storey buildings with CRBFs and BRBFs

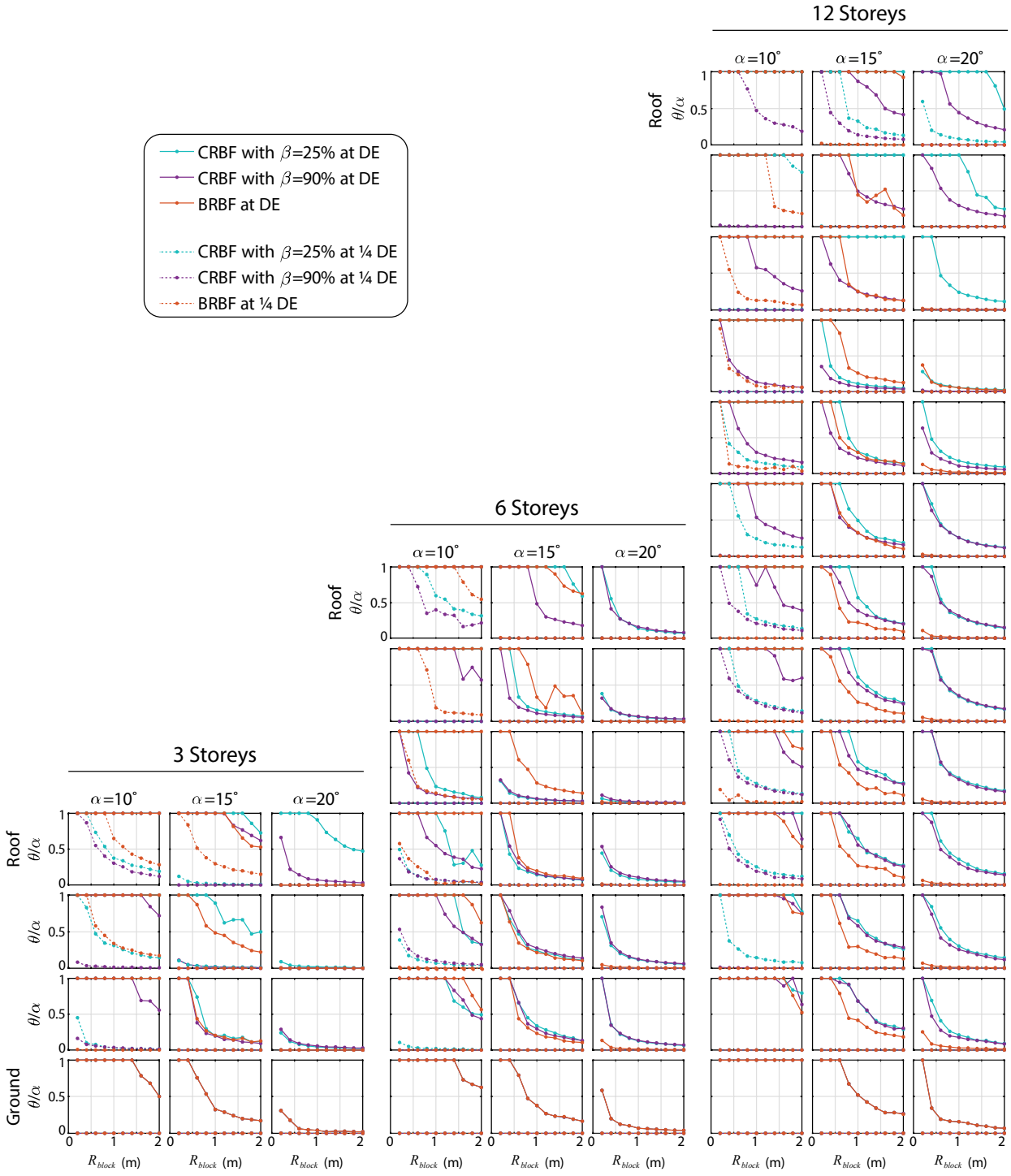

Figure 11 Median rocking spectra for unanchored slender components in the three-, six-, and 12-storey buildings with CRBFs and BRBFs

When comparing the two CRBF designs at each height, rocking component performance in the β = 90% CRBF was typically similar to or better than that in the β = 25% CRBF for the three-storey and 12-storey structures. However, for the six-storey CRBFs, rocking component performance was very similar between the two designs. This aligns with the previous observations of anchored and sliding component performance that the amount of supplemental energy dissipation provided in the base rocking joint design does not seem to have a significant impact on nonstructural component performance, whereas the rocking moment and stiffness of the frame likely play a larger role.

Similar to sliding component displacements, the peak rotations of rocking components do not seem to be well correlated with PFA, with the possible exception of stockier rocking components.

At ¼ DE level, rocking was negligible at all floors for almost all rocking component slenderness angles and sizes, except for the smallest blocks with $\alpha = 10°$ at some floor levels, with better performance in the CRBFs than in the BRBF.

EFFECT OF CRBF IMPACT ON NONSTRUCTURAL COMPONENT DEMANDS

One concern for nonstructural component performance in CRBFs is whether the CRBF hysteretic response transferring from a low lateral stiffness during rocking to a high lateral stiffness after impact can lead to a spike in the lateral floor accelerations or sliding/rocking component response [Wiebe and Christopoulos 2010; Buchanan et al. 2011; Lin et al. 2012]. To study this concern, Figure 12 shows the floor acceleration response and pseudo-acceleration response for anchored components with periods of 0.15 s and 0.44 s in the three-storey β = 25% CRBF building during the Superstition Hills ground motion (Poe Road recording station). The two anchored component natural periods coincided with local peaks in the floor spectra near the first- and second-mode periods of the CRBF. This ground motion was just under the 84th percentile in terms of PFA at the roof level and was chosen in order to assess a ground motion with significant floor accelerations while also having clearly defined cycles of CRBF impact. Vertical lines are plotted to denote moments of impact of the rocking frame on its foundation.

The responses show that the floor accelerations and pseudo-accelerations of the anchored components did not experience any significant spikes following CRBF impact, but rather exhibited similar magnitudes and frequencies before and after. Figure 12 also shows the effect of frame impact on a sliding component with μ = 0.2, a friction coefficient that was deemed low enough to produce a marked amount of sliding. Again, at each floor level there did not seem to be any significant changes in either the displacement or velocity response of the sliding component after impact of the frame. Finally, the rotations of three rocking components of slenderness $\alpha = 15°$ varying in size from R_{block} = 0.6 m to 1.0 m are also plotted for a wider time range in Figure 12. For the rocking components that did not overturn, the results did not show any notable changes in the magnitudes or rate of increase of the rocking rotations immediately after CRBF impact compared to the general magnitude and frequency of the rotation response prior to impact.

CONCLUSIONS AND RECOMMENDATIONS

This study evaluated the demands on anchored and unanchored (sliding and rocking) nonstructural components in buildings with CRBFs and compared them to those in buildings with BRBFs. Nonlinear time-history analyses were conducted on three-, six-, and 12-storey buildings, each with three different lateral force-resisting systems: two CRBF designs, differing in supplemental energy dissipation and frame stiffness, and one BRBF. Because nonstructural components can be drift-sensitive or acceleration-sensitive, the effective force modification factor of the designs was iterated until the median peak interstorey drifts were within 5% of the target design interstorey drift of 1.5%, thus suggesting similar demands on drift-sensitive components. The structural results showed that the CRBF frame members were capacity protected from elastic buckling at the 84th-percentile level in almost all cases, such that models with linear elastic frame elements could be relied on for calculating median demands. The residual drift performance was much better in the CRBFs, which self-centred after the design earthquake level events, whereas the BRBFs experienced median residual drifts of around 0.35% to 0.4%, with many ground motions causing residual drifts greater than 0.5%.

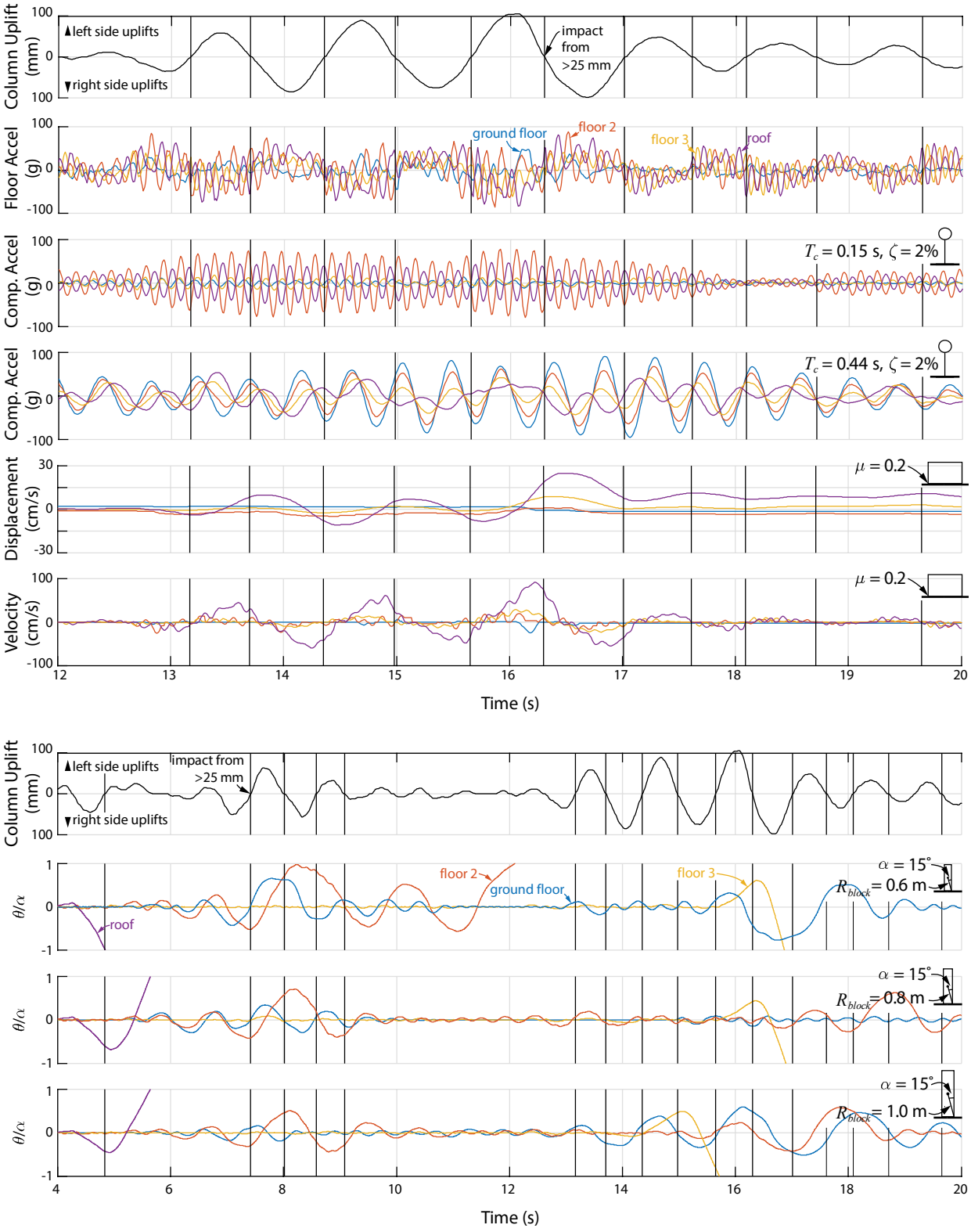

Figure 12 Three-storey CRBF with β=25%: column uplift, floor acceleration, attached component, sliding component, and rocking component responses during Superstition Hills, Poe Road ground motion

Considering the demands on rigid acceleration-sensitive anchored nonstructural components (periods of less than 0.06 s), the CRBFs experienced an amplification of the peak ground acceleration at most floors at the design earthquake intensity because of the elastic response of the frame members, whereas the BRBF peak floor accelerations were lower than the peak ground acceleration due to BRB yielding. For all building heights, the distribution of peak floor accelerations generally followed the shape of the third mode in the CRBFs but the first mode in the BRBFs. At lower ground motion intensities, the PFAs became similar between the two systems and were magnified relative to the PGAs in both systems. The PFAs were generally not predictive of the demands on other considered non-structural components.

For more flexible acceleration-sensitive anchored nonstructural components, the downside of the intended elastic response in the CRBF members was large, concentrated peaks in the floor spectra near the rocking higher-mode periods. These spectral peaks at the design earthquake level were much larger in the CRBFs than in the BRBFs, which had a capping and spreading effect over wider ranges of periods due to the brace yielding. The floor spectra magnitudes generally became similar or larger in the BRBF at longer periods, relevant for isolated components. At lower earthquake intensities, where the BRBF did not yield significantly, the floor spectra magnitudes were more alike between the two systems. However, the spectral accelerations peaked near the higher-mode periods, which were generally closer to the range of relevant natural periods for anchored components in the buildings with CRBFs than with BRBFs, which were more flexible. The concentration and magnitudes of these peaks compared to the BRBF floor spectra suggested that the acceleration response was likely driven by the lack of yielding in the CRBFs, rather than the CRBFs experiencing a significantly larger participation of higher modes compared to the BRBF.

Considering unanchored sliding components, the sliding displacements and velocities at the DE level were also generally lower in the BRBFs than the CRBFs. This was consistent with the differences in peak floor accelerations between the two systems, although at friction coefficients less than 0.2, the sliding displacements and velocities were much closer between the two systems. At ¼ DE level, sliding component demands were similar between the two systems, although these demands were negligible for components with friction coefficients greater than 0.2.

In contrast to the performance of anchored components and sliding components, the performance of unanchored rocking components was relatively similar between the two systems at the DE level. For the more slender components, demands in the buildings with CRBFs were sometimes lower than in the buildings with BRBFs, whereas the stockiest considered rocking components ($\alpha = 20°$) experienced lower rocking rotations in the buildings with BRBFs. At the ¼ DE level, the stockier rocking components ($\alpha = 15°$ and $20°$) experienced negligible rocking response, whereas the slender rocking components ($\alpha = 10°$) overturned for some of the smallest sized components.

To better understand the driving influences for nonstructural component demands in CRBFs, nonlinear-time history analyses were repeated for the two CRBF base rocking joint designs, which varied in rocking moment and supplemental energy dissipation, using the same frame members for both CRBFs. The results suggested that the amount of energy dissipation provided in the CRBF base rocking joint design had only a minimal effect on the floor spectra magnitudes, which were most influenced by the higher-mode response of the frame and by the base rocking moment.

There was no indication that the transition of the system transferring from a low lateral stiffness during rocking to a high lateral stiffness at column impact led to any spiking effects in the floor accelerations, nor any noticeable changes in nonstructural component responses.

Although this study showed that the amount of energy dissipation provided has little influence on floor acceleration demands when considering CRBFs of similar stiffness and rocking moment, increasing the amount of energy dissipation reduced the required base rocking moment to achieve the target displacements and the frame member capacity design forces, both of which reduce the demands on nonstructural components. Therefore, the recommendation to a CRBF designer considering the performance of nonstructural components is that the lowest demands are likely to be achieved by designing with the most flexible frame and lowest rocking moment that are possible while still meeting the design criteria related to interstorey drift limits, frame member strength, and margin against collapse. This is best done by maximizing the energy dissipation provided. Even when doing this, demands on nonstructural components can be relatively high, and thus a potential area of future study is developing mitigation strategies for reducing demands on nonstructural components in CRBFs while maintaining the structural performance

of the system. The use of multiple mechanisms, which has been shown to reduce structural demands caused by higher mode effects [Wiebe et al. 2013], may be beneficial in this regard.

ACKNOWLEDGMENTS

The financial support of the Natural Sciences and Engineering Research Council of Canada (NSERC), as well as the Early Researcher Award from the Ontario Ministry of Economic Development, Job Creation and Trade, is gratefully acknowledged.

REFERENCES

American Institute of Steel Construction (AISC). [2016] *Specification for Structural Steel Buildings*, ANSI/AISC Standard 360-16, Chicago, IL, USA.

American Institute of Steel Construction (AISC). [2016] *Seismic Provisions for Structural Steel Buildings*, ANSI/AISC Standard 341-16, Chicago, IL, USA.

American Society of Civil Engineers (ASCE). [2016] *Minimum Design Loads and Associated Criteria for Buildings and Other Structures*, ASCE/SEI Standard 7-16, Reston, VA, USA.

Applied Technology Council. [2009] *Quantification of Building Seismic Performance Factors*, FEMA Report P695, Prepared for the Federal Emergency Management Agency, Washington, DC, USA.

Bao, Y., Konstantinidis, D. [2020]. "Dynamics of a sliding-rocking block considering impact with an adjacent wall." *Earthquake Engineering and Structural Dynamics*, in-press.

Buccella, N. [2019] "Nonstructural component demands in buildings with controlled rocking steel braced frames," *M.A.Sc. Thesis*, McMaster University, Hamilton, Ontario, Canada.

Buchanan, A.H., Bull, D., Dhakal, R., MacRae, G., Palermo, A., Pampanin, S. [2011] "Base Isolation and Damage-Resistant Technologies for Improved Seismic Performance of Buildings," *Royal Commission of Inquiry into Building Failure Caused by the Canterbury Earthquakes: Research Report 2011-02*, Department of Civil and Natural Resources Engineering, University of Canterbury, Christchurch, New Zealand.

Chaudhuri, S.R., Hutchinson, T.C. [2006] "Fragility of Bench-Mounted Equipment Considering Uncertain Parameters," *Journal of Structural Engineering*, Vol. 132(6), pp. 884-898.

Dar, A., Konstantinidis, D., El-Dakhakhni, W. W. [2016] "Evaluation of ASCE 43-05 seismic design criteria for rocking objects in nuclear facilities," *Journal of Structural Engineering*, Vol. 142, No. 11, 04016110.

Dyanati, M., Huang, Q., Roke, D. [2014] "Structural and Nonstructural Performance Evaluation of Self-Centering Concentrically Braced Frames Under Seismic Loading," *Proceedings of ASCE 2014 Structures Congress*, Boston, MA, USA.

Eatherton, M.R., Hajjar, J.F. [2010] "Large-Scale Cyclic and Hybrid Simulation Testing and Development of a Controlled-Rocking Steel Building System with Replaceable Fuses," *NSEL Report NSEL-025*, Department of Civil and Environmental Engineering, University of Illinois at Urbana-Champaign, USA.

Eatherton, M.R., Ma, X., Krawinkler, H., Mar, D., Billington, S., Hajjar, J., Deierlein, G. [2014] "Design concepts for controlled rocking of self-centering steel-braced frames," *Journal of Structural Engineering*, Vol. 140(11), No. 4014082.

Filiatrault, A., Uang, C.-M., Folz, B., Christopoulos, C., Gatto, K. [2001] "Reconnaissance report of the February 28, 2001 Nisqually (Seattle-Olympia) earthquake," *Report No. SSRP-2001/02 for the Structural Systems Research Project*, University of California, San Diego, La Jolla, USA.

Gledhill, S.M., Sidwell, G.K., Bell, D.K. [2008] "The Damage Avoidance Design of tall steel frame buildings - Fairlie Terrace Student Accommodation Project, Victoria University of Wellington.," *Proceedings of the 2008 NZSEE Conference,* Wairakei, New Zealand.

Housner, G.W. [1963] "The behavior of inverted pendulum structures during earthquakes," *Bulletin of the Seismological Society of America*, Vol. 53, No. 2, pp. 403-417.

Konstantinidis, D., Makris, N. [2009] "Experimental and analytical studies on the response of freestanding laboratory equipment to earthquake shaking," *Earthquake Engineering & Structural Dynamics*, Vol. 38, No. 6, pp. 827-848.

Konstantinidis, D., Makris, N. [2010] "Experimental and analytical studies on the response of 1/4-scale models of freestanding laboratory equipment subjected to strong earthquake shaking," *Bulletin of Earthquake Engineering*, Vol. 8, No. 6, pp. 1457-1477.

Konstantinidis, D., Nikfar, F. [2015] "Seismic response of sliding equipment and contents in base-isolated buildings subjected to broadband ground motions," *Earthquake Engineering & Structural Dynamics*, Vol. 44, No. 6, pp. 865-887.

Latham, D.A., Reay, A.M., Pampanin, S. [2013] "Kilmore Street Medical Centre: Application of a Post-Tensioned Steel Rocking System," *Proceedings of the Steel Innovations Conference 2013*, Christchurch, New Zealand.

Lin, S.L., MacRae, G.A., Dhakal, R.P., Yeow, T.Z. [2012] "Contents Sliding Response Spectra," *Proceedings of 15th World Conference on Earthquake Engineering*, Lisboa, Portugal.

Lin, S.L., MacRae, G.A., Dhakal, R.P., & Yeow, T.Z. [2015]. "Building contents sliding demands in elastically responding structures," *Engineering Structures*, Vol. 86, pp. 182-191.

MATLAB. [2017] Version 2017b, *The Language of Technical Computing*, The Mathworks, Inc.: Natick, USA.

Ma, X., Krawinkler, H., Deierlein, G. [2010] "Seismic Design and Behavior of Self-Centering Braced Frame with Controlled Rocking and Energy-Dissipating Fuses," *Blume Earthquake Engineering Center Report 174*, Department of Civil and Environmental Engineering, Stanford University, USA.

Makris, N., Konstantinidis, D. [2003] "The rocking spectrum and the limitations of practical design methodologies," *Earthquake Engineering & Structural Dynamics*, Vol. 32, No. 2, pp. 265-289.

McCormick, J., Aburano, H., Ikenaga, M., Nakashima, M. [2008] "Permissible residual deformation levels for building structures considering both safety and human elements," *Proceedings of 14th World Conference on Earthquake Engineering*, Beijing, China.

Miranda, E., Mosqueda, G., Retamales, R., Pekcan, G. [2012] "Performance of non-structural components during the 27 February 2010 Chile earthquake," *Earthquake Spectra*, Vol. 28, No. S1, pp. S453-S471.

Mottier, P., Tremblay, R., Rogers, C. [2018] "Seismic retrofit of low-rise steel buildings in Canada using rocking steel braced frames," *Earthquake Engineering & Structural Dynamics*, Vol. 47, No. 2, pp. 333-355.

Nikfar, F., N.A., Konstantinidis, D. [2017] "Effect of the Stick-Slip Phenomenon on the Sliding Response of Objects Subjected to Pulse Excitation," *Journal of Engineering Mechanics*, Vol. 143(4), No. 04016122.

Pacific Earthquake Engineering Research Center. [2015] Open System for Earthquake Engineering Simulation v2.4.4, [Computer Software].

Pollino, M. [2014] "Seismic design for enhanced building performance using rocking steel braced frames," *Engineering Structures*, Vol. 83, pp. 129-139.

Roke, D., Sause, R., Ricles, J.M., Chancellor, N.B. [2010] "Damage-Free Seismic-Resistant Self-Centering Concentrically-Braced Frames," *ATLSS Report 10-09*, Lehigh University, USA.

Saxey, B., Daniels, M. [2014] "Characterization of overstrength factors for buckling restrained braces," *Proceedings of Australasian Structural Engineering Conference*, Auckland, New Zealand.

Steele, T.C. [2019] "Ultimate limit states in Controlled Rocking Steel Braced Frames," *Ph.D. Thesis*, McMaster University, Hamilton, Ontario, Canada.

Steele, T.C., Wiebe, L. [2016] "Dynamic and equivalent static procedures for capacity design of controlled rocking steel braced frames," *Earthquake Engineering & Structural Dynamics*, Vol. 45, No. 14, pp. 2349-2369.

Steele, T.C., Wiebe, L. [2017] "Collapse risk of controlled rocking steel braced frames with different post-tensioning and energy dissipation designs," *Earthquake Engineering & Structural Dynamics*, Vol. 46, No. 13, pp. 2063-2082.

Steele, T.C., Wiebe, L. [2020] "Large-scale experimental testing and numerical modelling of floor-to-frame connections for controlled rocking steel braced frames," *Journal of Structural Engineering*, Under Review.

Taghavi, S., Miranda, E. [2003] "Response Assessment of Nonstructural Building Elements," *Report PEER 2003/05,* Pacific Earthquake Engineering Research Center, University of California, Berkeley, USA.

Van Engelen, N., Konstantinidis, D., Tait, M. [2016] "Structural and nonstructural performance of a seismically isolated building using stable unbonded fiber-reinforced elastomeric isolators," *Earthquake Engineering & Structural Dynamics*, Vol. 45, No. 3, pp. 421-439.

Wiebe, L., Christopoulos, C. [2010] "Characterizing acceleration spikes due to stiffness changes in nonlinear systems," *Earthquake Engineering & Structural Dynamics*, Vol. 39, pp. 1653-1670.

Wiebe, L., Christopoulos, C., Tremblay, R., Leclerc, M. [2013] "Mechanisms to limit higher mode effects in a controlled rocking steel frame. 2: Large-amplitude shake table testing," *Earthquake Engineering & Structural Dynamics*, Vol. 42, pp. 1069-1086.

Wiebe, L., Christopoulos, C. [2015a] "Performance-Based Seismic Design of Controlled Rocking Steel Braced Frames. I: Methodological Framework and Design of Base Rocking Joint," *Journal of Structural Engineering*, Vol. 141(9), No. 04014226.